ELSEVIER

Journal of Alloys and Compounds 237 (1996) 9–19

Journal of ALLOYS AND COMPOUNDS

The magnetic structures of the mixed layer pnictide oxide compounds $Sr_2Mn_3Pn_2O_2$ (Pn = As, Sb)

Stephanie L. Brock[a], N.P. Raju[b], J.E. Greedan[b,*], Susan M. Kauzlarich[a,*]

[a] *Department of Chemistry, University of California, Davis, CA 95616, USA*

[b] *Institute for Materials Research, McMaster University, Hamilton, Ontario L8S 4M1, Canada*

Received 16 June 1995; in final form 14 September 1995

Abstract

Neutron powder diffraction results are reported for the compounds $Sr_2Mn_3Pn_2O_2$ (Pn = As, Sb), and the magnetic structures are determined. The chemical structure can be described as a 1:1 intergrowth of $Mn_2Pn_2^{2-}$ layers of the $BaAl_4$ type with MnO_2^{2-} layers isostructural with the CuO_2 planes found in cuprate superconductors. The Sr^{2+} cations separate the two layers. Two independent magnetic sublattices exist, Mn(1) and Mn(2), associated with the MnO_2^{2-} and $Mn_2Pn_2^{2-}$ layers respectively. Both sublattices have tetragonal symmetry, Mn(2) being primitive and Mn(1) being centered. The interlayer spacing within each sublattice is about 10 Å and between the sublattices it is about 5 Å. Owing to the centering of the Mn(1) sublattice, interactions between the nearest MnO_2^{2-} layers cancel, as do interactions between the Mn(1) and Mn(2) sublattices. The Mn(2) sublattice is found to order at the relatively high temperatures of about 340 K (As) and 300 K (Sb) in a type G_z structure, $\boldsymbol{k} = (0\,0\,0)$ with a saturation moment of 3.4 μ_B at 4 K. At low temperatures new reflections of magnetic origin appear which can be assigned to the Mn(1) sublattice, but the details are different for each compound. The Mn(1) moments for $Sr_2Mn_3Sb_2O_2$ order below 65 K with $\boldsymbol{k} = (1/2\,1/2\,0)$ along $\langle 100 \rangle$, i.e. normal to the Mn(2) spins, with a significantly larger moment of 4.2 μ_B. In $Sr_2Mn_3As_2O_2$ one sees much weaker reflections below 75 K, the most prominent of which shows a Warren line shape characteristic of two-dimensional correlations only. Thus it appears that the Mn(1) sublattice may not order in the long range sense down to 4 K in $Sr_2Mn_3As_2O_2$. The properties of the individual sublattices of these manganese pnictide oxides are compared with similar magnetic sublattices of other compounds.

Keywords: Neutron diffraction; Magnetic structure; Antiferromagnetism; Layered compounds; Pnictide oxide compounds

1. Introduction

Many layered compounds can be grouped into categories according to the type of building block units employed in the structure. Properties associated with a particular building block can be modified by incorporation of different layers to create a variety of useful materials. One example is the huge number of perovskite-based compounds. These include the aurivillius phases, which consist of alternating perovskite and fluorite blocks, and Ruddlesden–Popper phases which have NaCl-type blocks alternating with the perovskite units [1]. Another common building block in layered compounds is the $BaAl_4$ unit [2]. The structure consists of two different Al environments: a tetrahedral site (Al(1)), and an antiprismatic site (Al(2)). This unit appears in many different ternary layered structure types, among them the $ThCr_2Si_2$ and CeFeSi structure types [2]. In many cases, the tetrahedral site is occupied by a transition metal cation and the antiprismatic site by a larger main group anion. There is a well-documented versatility with respect to size and oxidation state of the elemental components, which results in a huge number of compounds with a wide variety of properties. Compounds containing $BaAl_4$-type units which have received a lot of interest include the superconducting boro-carbides $LnNi_2B_2C$ [3] (Ln = rare earth metal) and the rare earth compounds of the $ThCr_2Si_2$ structure type [4–10].

We have been studying a series of compounds $A_2Mn_3Pn_2O_2$ (A = Sr, Ba; Pn = P, As, Sb, Bi) [11,12] which couple the $BaAl_4$ unit with MO_2 planar units, an important structural feature in many layered oxides and a critical component in the high T_c superconduct-

* Corresponding author.

SSDI 0925-8388(95)02066-7

ing copper oxide compounds. Indeed it is the variety and interest in the properties of the two independent units that has prompted our investigation of these compounds in which they are combined into a single structure [13,14]. Our interest is in developing an understanding of structure–property relationships in these materials and the synthesis of new compounds of this structure type. Magnetic susceptibility measurements have been reported on the barium analogs and they suggest the presence of low-dimensional antiferromagnetic coupling. However, it is difficult to establish the contribution to the magnetism from the two unique sites in these compounds from magnetic susceptibility measurements alone. Thus, neutron diffraction measurements have been obtained on two members of the series, $Sr_2Mn_3Sb_2O_2$ and $Sr_2Mn_3As_2O_2$, in an effort to determine the magnetic structure of these compounds. This paper will describe magnetic models for the two compounds and compare them with structurally related materials.

2. Experimental procedure

2.1. Materials

SrO was prepared from thermal decomposition of $SrCO_3$ (Johnson Matthey, 99.999%) under vacuum (1000 °C, 48 h). Mn flake (Johnson Matthey, 99.9%) was etched with 15 %vol. HNO_3 in methanol and rinsed with acetone before use. As and Sb (Johnson Matthey, 99.9999%) were used as-received without further purification. All materials were handled in a drybox under argon and ground, using a mortar and pestle, before use.

2.2. Synthesis

$Sr_2Mn_3As_2O_2$ and $Sr_2Mn_3Sb_2O_2$ were prepared by combining stoichiometric amounts of SrO, Mn, and As or Sb, grinding the reactants together in a mortar and pestle and pressing them into a pellet (5000 lbf in^{-2}). The pellets were then placed in an alumina boat and sealed in a fused silica ampoule under 0.5 atm of argon. The samples were heated to 1000°C by 30°C h^{-1}, left for 1 week, then rapidly cooled. Reactions were performed on a 1 g scale.

2.3. Neutron diffraction measurements

Powder neutron diffraction data were obtained from the DUALSPEC diffractometer at the Atomic Energy of Canada Limited facility in Chalk River, Ontario. Approximately 5 g each of $Sr_2Mn_3As_2O_2$ and $Sr_2Mn_3Sb_2O_2$ were loaded, under a helium atmosphere, into vanadium sample cells and sealed with an indium gasket. Neutrons of wavelength 2.508 Å, obtained from the reactor source using a silicon crystal (311) monochromator and a take-off angle of 99.5°, were employed. A top-loading liquid helium cryostat was used for data collection between 4 and 275 K. High temperature data were obtained, up to 430 K, with a furnace inset. The data were analyzed using the FULLPROF software system [15].

3. Results

The compounds $Sr_2Mn_3Pn_2O_2$ crystallize in the tetragonal space group $I4/mmm$ with lattice parameters $a = 4.1459(2)$, $c = 18.856(2)$ Å (Pn = As) and $a = 4.2599(4)$, $c = 20.093(3)$ Å (Pn = Sb) [11,12]. The structure, illustrated in Fig. 1, consists of alternating $Mn_2Pn_2^{2-}$ and MnO_2^{2-} layers separated by the Sr^{2+} cations. The $Mn_2Pn_2^{2-}$ layers are of the $BaAl_4$ structure type. They are built of a square planar Mn network alternatively capped above and below the plane by Pn atoms to form an edge sharing $MnPn_{4/4}$ tetrahedral network. The MnO_2^{2-} layers are composed of $MnO_{2/4}^{2-}$ square planes and are isostructural to CuO_2 layers in the high T_c superconductors. The Pn atoms of the $Mn_2Pn_2^{2-}$ layers point toward the Mn atoms of the interleaving MnO_2^{2-} layers. This Mn–Pn interplanar distance is on the order of a van der Waals interaction [16].

There are two different Mn positions in the

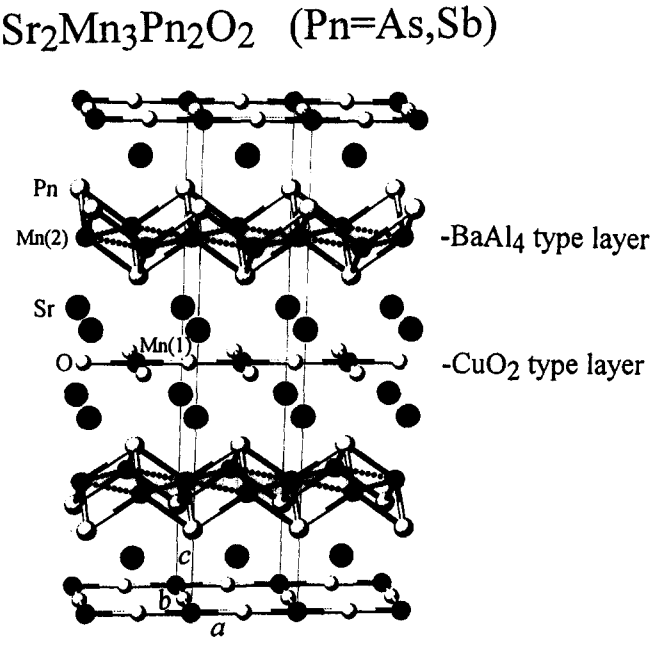

Fig. 1. A view of the structure of $Sr_2Mn_3Pn_2O_2$ (Pn = As, Sb) with the unit cell indicated. The structure is an intergrowth of $BaAl_4$-type layers ($Mn_2Pn_2^{2-}$) and CuO_2-type layers (MnO_2^{2-}).

$Sr_2Mn_3Pn_2O_2$ structure. The Mn atoms of the MnO_2^{2-} layers, Mn(1), sit on the 2a sites and those of the $Mn_2Pn_2^{2-}$ layers, Mn(2), are on the 4d sites. From the figure it is clear that both sublattices have the expected tetragonal symmetry, but the Mn(1) sublattice is centered while that of Mn(2) is primitive. The interlayer distances within each sublattice are in the 9–10 Å range and those between sublattices are in the 4.5–5 Å range. Owing to geometric differences, if the coupling within the two sublattices is antiferromagnetic, Mn(1) will have an equal number of neighbours in the Mn(2) lattice with spin up as with spin down, resulting in no net interaction. This will also be the case for the coupling of one Mn(1) layer to its nearest Mn(1) layer, due to the centering of the Mn(1) lattice. Thus, for the Mn(1) sublattice, antiferromagnetic interactions will cancel in the c dimension to the nearest Mn(1) layer as well as to the Mn(2) layers. In contrast, interactions between the Mn(2) layers along c are not expected to cancel based on symmetry.

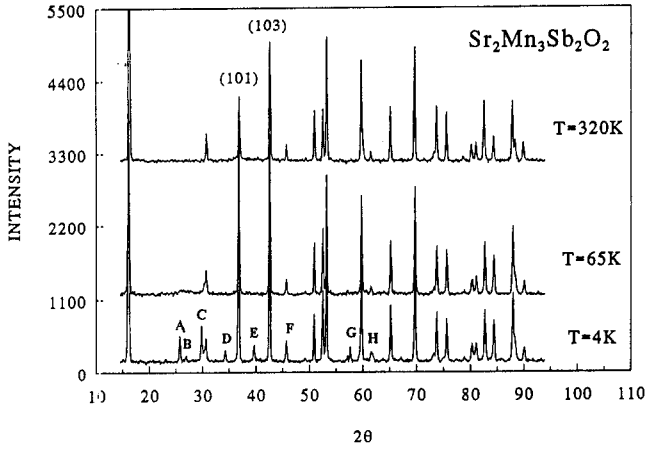

Fig. 2. Neutron diffraction profiles at 4, 65, and 320 K for $Sr_2Mn_3Sb_2O_2$.

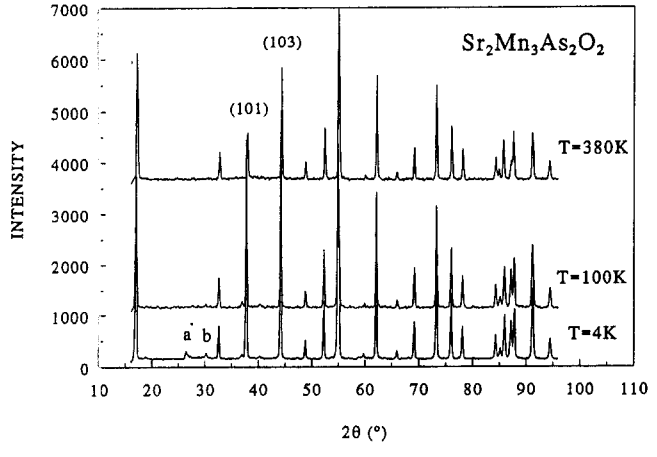

Fig. 3. Neutron diffraction profiles at 4, 100, and 380 K for $Sr_2Mn_3As_2O_2$.

Neutron diffraction profiles for $Sr_2Mn_3Sb_2O_2$ and $Sr_2Mn_3As_2O_2$ are presented in Figs. 2 and 3 respectively. Upon examination of the powder patterns for both materials over the entire temperature range investigated, it is apparent that three distinct regions exist. In region I, $T > 300$ K for Sb or $T > 340$ K for As, the pattern could be fit very well with a model including only the crystal structure details, i.e. no magnetic component. In region II, $65\,\mathrm{K} < T < 300\,K$ (*Sb*), $75\,\mathrm{K} < T < 340\,\mathrm{K}$ (As), the (101) and (103) reflections are significantly enhanced, but no new reflections appear. At low temperature (region III) new reflections, which cannot be indexed on the chemical cell, appear for both compounds.

Refinement results for region I are included in Tables 1 and 2 for $Sr_2Mn_3Sb_2O_2$ and $Sr_2Mn_3AsO_2$ respectively. Apart from small decreases in cell constants and thermal parameters as the temperature is lowered, there are no significant changes in the basic crystal structure of these compounds down to 4 K.

Concerning region II, the enhanced reflections (101) and (103) follow the rule $h + k =$ odd, $l =$ odd. This parallels the situation found for $BaMn_2P_2$ which contains only the Mn(2) sublattice. As with that compound [17,18], the neutron powder pattern could be fit assuming a type G_z magnetic component, i.e. both intra- and interlayer nearest moments antiparallel, with the preferred moment direction parallel to c, associated only with the Mn(2) sites. Typical fits for region II are shown for both compounds in Figs. 4 and 5 and refinement results are summarized in Tables 1 and 2. The temperature dependence of the Mn(2) moment extracted from these fits is displayed for both materials in Fig. 6. The data indicates that transitions to a long range ordered state occur below about 300 and 340 K for the Sb and As compounds respectively.

Turning to region III, one sees significant differences between the two compounds, as indicated in Figs. 2 and 3. For $Sr_2Mn_3Sb_2O_2$ as many as eight relatively well-defined reflections, labeled A–H, are seen, whereas the set of reflections for the corresponding As phase, labeled a and b, are much weaker and very different in appearance.

The new reflections for $Sr_2Mn_3Sb_2O_2$ can all be indexed on a new cell with dimensions $a_{MAG} = \sqrt{2}a$, $c_{MAG} = c$, as shown in Table 3, and the reflection condition is $h + k =$ odd. This magnetic cell and the observed indices are the same as those normally seen for ordered K_2NiF_4 compounds, which also possess the centered tetragonal magnetic sublattice of Mn(1). Trial refinements based on this model were carried out using the software package FULLPROF [15]. The crystal and complete magnetic structure, for both Mn(1) and Mn(2), has space group symmetry $Am2'm'$ and can be described in $P222$ where Mn(1) is 1a and 1f (+) and 1e and 1g (−) while Mn(2) occupies 4u with coordi-

Table 1
Results of combined crystal structure and magnetic structure refinements for $Sr_2Mn_3Sb_2O_2$ between 340 and 4 K

	340 K	330 K	320 K	300 K	250 K	225 K	200 K	150 K	100 K	65 K	60 K	50 K	30 K	4 K
Sr (0 0 z)														
z	0.4208(5)	0.4212(5)	0.4209(5)	0.4210(5)	0.4214(5)	0.4214(5)	0.4209(5)	0.4209(6)	0.4207(4)	0.4208(5)	0.4212(4)	0.4205(4)	0.4206(4)	0.4210(3)
B_{iso}(Å^2)	1.6(4)	1.9(5)	1.7(4)	1.8(4)	1.5(5)	1.6(5)	1.3(5)	1.2(5)	1.1(3)	0.6(5)	1.1(3)	1.0(4)	0.9(3)	1.2(3)
Mn1 (0 0 0)														
B_{iso}(Å^2)	0.2(8)	0.4(9)	0.8(9)	0.5(9)	−0.4(9)	1.1(9)	0.3(9)	−0.9(9)	1.0(7)	−1.7(9)	−1.7(6)	1.6(6)	−0.7(6)	−0.9(4)
Moment (μ_B)	—	—	—	—	—	—	—	—	—	—	2.5(2)	3.4(2)	3.9(2)	4.2(3)
Mn2 (0 1/2 1/4)														
B_{iso}(Å^2)	2.1(7)	2.7(7)	2.4(7)	2.7(7)	1.7(7)	2.4(7)	2.0(7)	1.5(7)	1.7(5)	1.7(7)	1.7(4)	1.7(5)	2.0(4)	1.8(3)
Moment(μ_B)	0.5(4)	0.4(5)	0.5(4)	0.6(3)	2.5(1)	2.8(1)	2.9(1)	3.3(1)	3.5(1)	3.4(1)	3.5(1)	3.5(1)	3.6(1)	3.5(1)
Sb (0 0 z)														
z	0.163(1)	0.1635(7)	0.1633(7)	0.1634(7)	0.163(1)	0.1619(8)	0.1629(8)	0.1624(8)	0.1622(6)	0.1621(8)	0.1625(5)	0.1624(6)	0.1626(6)	0.1622(4)
B_{iso}(Å^2)	1.0(4)	1.5(5)	1.1(4)	1.2(5)	0.8(5)	0.8(4)	0.6(4)	0.5(4)	0.1(3)	0.1(4)	0.3(3)	0.1(3)	0.1(3)	0.4(3)
O (0 1/2 0)														
B_{iso}(Å^2)	1.1(5)	0.8(5)	1.3(5)	1.5(5)	0.5(5)	0.5(5)	0.8(5)	0.4(5)	0.2(4)	−0.1(5)	0.2(3)	0.0(4)	0.3(4)	0.5(3)
a (Å)	4.2704(5)	4.2702(5)	4.2688(5)	4.2679(5)	4.2650(4)	4.2634(4)	4.2625(4)	4.2600(4)	4.2572(3)	4.2563(4)	4.2562(2)	4.2558(3)	4.2557(3)	4.2549(2)
c (Å)	20.177(3)	20.172(3)	20.166(3)	20.159(3)	20.139(2)	20.129(2)	20.179(2)	20.102(3)	20.087(2)	20.082(2)	20.079(2)	20.079(2)	20.077(2)	20.074(1)
Volume (Å^3)	367.942	367.822	367.487	367.190	366.332	365.877	365.559	364.815	364.076	363.794	363.736	363.680	363.604	363.418
R_{wp}	11.8	12.2	12.0	11.9	11.7	11.4	11.8	11.7	11.8	11.9	11.7	11.8	11.5	11.5
R_{exp}	4.3	4.3	4.3	4.2	4.4	4.4	4.4	4.4	4.4	4.4	5.6	5.6	5.9	6.1
χ^2	7.6	8.2	7.9	7.9	7.0	6.8	7.2	7.2	7.3	7.4	4.4	4.4	3.8	3.6
Bragg R factor	4.61	5.30	4.83	4.86	4.80	4.6	5.24	4.48	5.23	4.36	4.76	4.5	5.22	5.15
R—F factor	3.39	4.13	3.68	3.60	3.06	3.0	4.01	3.19	3.58	3.00	3.70	3.13	3.63	3.54
Mn(1) magnetic R factor	—	—	—	—	—	—	—	—	—	—	34.6	25.8	16.3	12.3
Mn(2) magnetic R factor	3.51	3.47	4.56	5.51	3.47	3.5	3.73	3.17	3.75	3.31	3.00	3.58	3.89	3.19

Table 2
Results of combined crystal structure and magnetic structure refinements for $Sr_2Mn_3As_2O_2$ between 380 and 4 K

	380 K	360 K	340 K	320 K	300 K	275 K	200 K	100 K	50 K	25 K	4 K
Sr (0 0 z)											
z	0.4140(2)	0.4139(2)	0.4139(5)	0.4142(4)	0.4140(3)	0.4135(3)	0.4137(3)	0.4137(3)	0.4137(3)	0.4138(3)	0.4136(3)
B_{iso}(Å^2)	0.8(3)	1.0(3)	0.8(6)	0.7(5)	0.8(5)	0.5(3)	0.3(3)	0.0(3)	0.4(3)	0.3(3)	0.1(3)
Mn1 (0 0 0)											
B_{iso}(Å^2)	0.5(4)	0.8(4)	0.4(8)	0.3(8)	0.2(7)	0.6(5)	0.4(5)	−0.2(5)	−0.5(5)	−0.05(5)	0.5(4)
Mn2 (0 1/2 1/4)											
B_{iso}(Å^2)	0.5(3)	1.1(3)	0.8(7)	0.6(6)	1.0(6)	1.5(4)	1.0(4)	0.5(4)	1.0(4)	0.6(4)	0.4(3)
Moment (μ_B)	0.5(2)	0.6(1)	0.6(3)	1.6(1)	2.0(1)	2.4(1)	2.9(1)	3.3(1)	3.4(1)	3.4(1)	3.4(1)
As (0 0 z)											
z	0.1693(3)	0.1691(3)	0.1692(6)	0.1691(5)	0.1690(5)	0.1696(3)	0.1699(4)	0.1693(4)	0.1691(3)	0.1691(4)	0.1691(3)
B_{iso}(Å^2)	0.8(2)	0.9(2)	0.8(5)	0.9(5)	0.9(4)	0.6(3)	0.4(3)	0.3(3)	0.5(2)	0.4(2)	0.1(2)
O (0 1/2 0)											
B_{iso}(Å^2)	0.9(3)	1.1(3)	0.8(5)	0.7(5)	0.7(5)	0.7(3)	0.7(3)	0.2(3)	0.4(3)	0.3(3)	0.1(3)
a(Å)	4.1541(2)	4.1531(2)	4.1521(5)	4.1512(4)	4.1500(4)	4.1494(2)	4.1455(2)	4.1418(1)	4.1411(5)	4.1409(2)	4.1407(2)
c(Å)	18.900(1)	18.891(2)	18.884(2)	18.876(2)	18.867(2)	18.859(1)	18.829(1)	18.789(1)	18.791(1)	18.789(2)	18.787(1)
Volume (Å^3)	326.160	325.856	325.566	325.273	324.928	324.720	323.575	322.479	322.233	322.166	322.108
R_{wp}	8.0	8.1	12.5	11.4	11.1	9.3	9.6	9.5	10.4	11.0	10.2
R_{exp}	5.4	5.4	4.3	4.3	4.3	5.2	5.2	5.1	5.0	5.0	5.0
χ^2	2.2	2.3	8.6	7.1	6.7	3.2	3.5	3.5	4.3	4.5	4.1
Bragg R factor	3.08	3.71	4.5	4.34	3.61	3.77	3.84	3.37	3.93	4.04	3.44
R–F factor	1.85	2.35	2.60	2.80	2.43	2.48	2.56	2.02	3.03	2.99	2.51
Mn(2) magnetic R factor	1.88	3.27	4.60	2.57	1.65	2.00	1.23	1.95	1.38	1.22	2.05

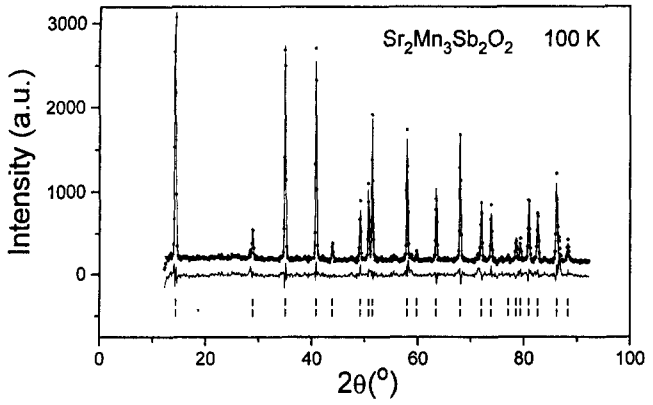

Fig. 4. A fit of the G-type magnetic model for the Mn(2) magnetic sublattice to the neutron diffraction data for $Sr_2Mn_3Sb_2O_2$ at 100 K. The data and fit are plotted on top and the difference plot and peak positions are indicated below.

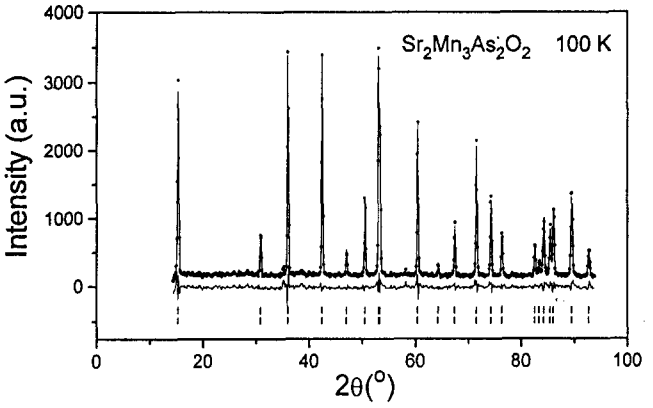

Fig. 5. A fit of the G-type magnetic model for the Mn(2) magnetic sublattice to the neutron diffraction data for $Sr_2Mn_3As_2O_2$ at 100 K. The data and fit are plotted on top and the difference plot and peak positions are indicated below.

nates $x = y = z = 3/4$ (+) and $x = y = z = 1/4$ (−). Refinements with the Mn(1) moment direction along ⟨001⟩, i.e. parallel to the existing G_z Mn(2) sublattice, or along ⟨110⟩ did not give a satisfactory fit, but a model with the moments along ⟨100⟩ refined readily. The magnetic moment and direction of Mn(1) from 4 to 60 K were refined without imposing any constraints. The refinement gives the moment direction as ⟨100⟩ with an error of +/−4° in the x–y plane and +/−2° out of the plane. This magnetic model for Mn(1) is illustrated in Fig. 7 along with the G_z Mn(2) magnetic sublattice. Fig. 8 shows the Rietveld fitting result at 4 K for $Sr_2Mn_3Sb_2O_2$ which incorporates both the Mn(1) and Mn(2) orderings, and the refinement details are given in Table 1. The R_{mag} values for the Mn(1) sublattice are large relative to R_{Bragg} and R_{mag} for Mn(2). This is due largely to the weakness of the Mn(1) magnetic reflections. The most intense Mn(1) peak is only 10% of the strongest structure peak and only 20% of the strongest Mn(2) line. In this light the value of 12.3% at 4 K is acceptable. It should be noted

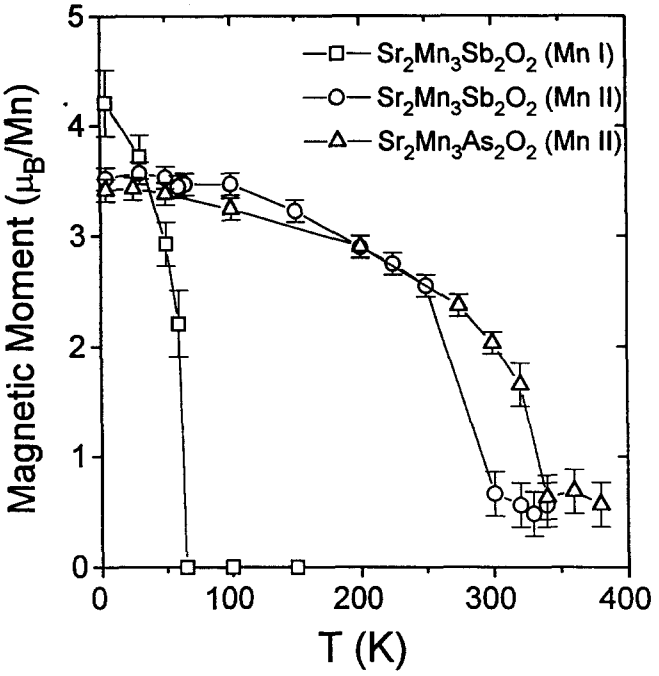

Fig. 6. A plot of the magnetic moment as a function of temperature for the Mn(2) magnetic sublattice of $Sr_2Mn_3Sb_2O_2$ and $Sr_2Mn_3As_2O_2$ and for the Mn(1) magnetic sublattice of $Sr_2Mn_3Sb_2O_2$.

Table 3
Positions of the magnetic reflections for $Sr_2Mn_3Sb_2O_2$ in region III

Peak	$2\theta_{obs}$(deg)[a]	$2\theta_{calc}$(deg)[b]	Indices[b]
A	23.95(1)	23.98	(100)
B	25.05(2)	25.05	(101)
C	28.00(1)	28.03	(102)
D	32.46(1)	32.44	(103)
E	37.84(1)	37.84	(104)
F	43.98(1)	43.95	(105)
G	55.88(7)	55.89	(211)
H	60.06(1)	60.08	(213)

[a] Observed 2θ values have been corrected for the zero point offset of 1.81°.
[b] Calculated 2θ values and indices are based on a magnetic cell $a_{MAG} = \sqrt{2}a$, $c_{MAG} = c$; $a_{MAG} = 6.026$ Å, $c_{MAG} = 20.101$ Å.

that the most prominent Mn(1) reflection, (012), is overlapped by the (1/2 1/2 1/2) magnetic reflection from an MnO impurity phase ($T_n = 116$ K). The data have been corrected for this overlap in arriving at the R_{mag} values listed in Table 1. The temperature dependence of the Mn(1) moment is compared with that of Mn(2) in Fig. 6 and is consistent with an ordering temperature of 65 K.

Returning to the low temperature results for the arsenic phase, we have already noted that at the magnification level of Fig. 3 there are only two prominent features, in sharp contrast to the case for $Sr_2Mn_3Sb_2O_2$. However, if this region is expanded, as in Fig. 9, it is possible to discern four additional very weak reflections, labeled c, d, e, and f.

The most prominent reflection, a, can be indexed as

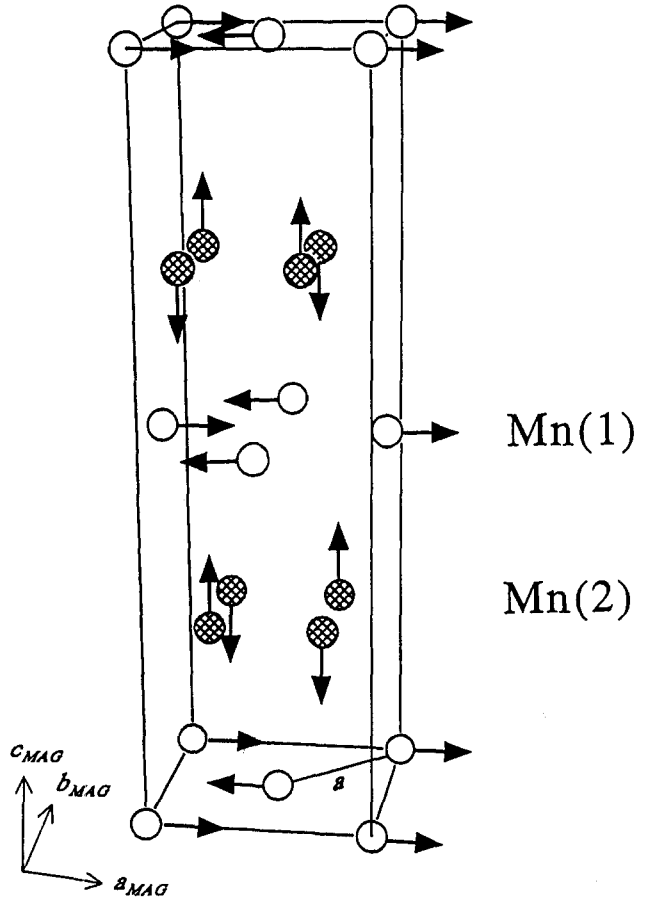

Fig. 7. Illustration of coupling within the Mn(1) (K_2NiF_4 type) and Mn(2) (G type) sublattices for $Sr_2Mn_3Sb_2O_2$ based on the cell $a_{MAG} = \sqrt{2}a$, $c_{MAG} = c$. The a dimension of the chemical cell is indicated.

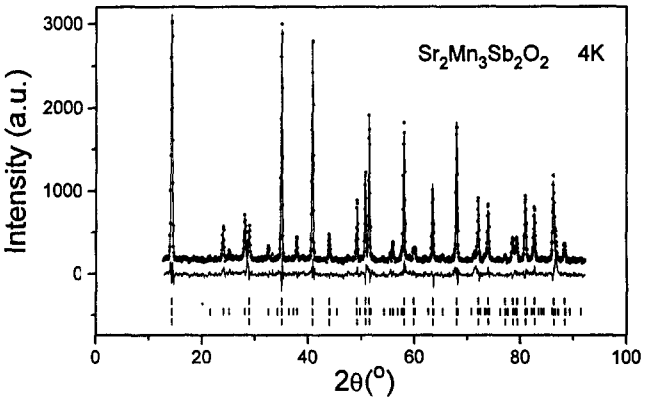

Fig. 8. Fit of both Mn(1) (K_2NiF_4-type model) and Mn(2) (G-type model) magnetic sublattices to the neutron diffraction data for $Sr_2Mn_3Sb_2O_2$ at 4 K. The data and fit are plotted on top and the difference plot and peak positions are indicated below.

(100) on an $a_{MAG} = \sqrt{2}a$, $c_{MAG} = c$ magnetic cell, analogous to the antimony compound. Unlike the pattern for the latter material, no reflections of the type (101) can be found for $Sr_2Mn_3As_2O_2$. Furthermore, the lineshape for (100) is of the Warren type

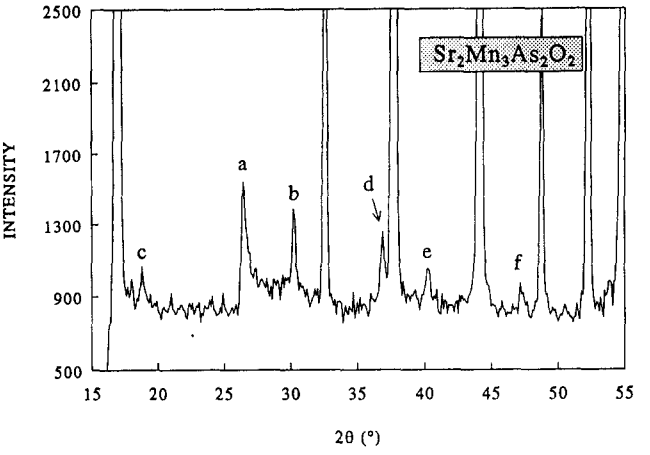

Fig. 9. An expanded view of the 4 K neutron diffraction profile for $Sr_2Mn_3As_2O_2$. The weak reflections ascribed to the Mn(1) magnetic sublattice are indicated by the letters a, c–h. The reflection labeled as b is the MnO (1/2 1/2 1/2) magnetic reflection.

[19]. Both these observations indicate that the (100) reflection arises from correlations which are two-dimensional. The second most prominent reflection, b, can be assigned as the (1/2 1/2 1/2) magnetic reflection of MnO, which is present as an impurity phase. Table 4 lists the positions, indices, relative integrated intensities and line widths of all reflections which cannot be assigned to MnO.

From Table 4 it is clear that about 90% of the new scattered intensity at 4 K arises from the (100) reflection. Thus, it is reasonable to assume that analysis of this feature will provide the most important information regarding the Mn(1) magnetic correlations in $Sr_2Mn_3As_2O_2$ which are, as noted, two-dimensional and thus of short range only. A fit of the (100) reflection to the Warren function is presented in Fig. 10. The parameters suggest a correlation length of about 540 Å at 4 K for the coupled spins. Fig. 11 shows the temperature dependence of the (100) reflection which is seen to broaden and collapse near 75 K. Note that the MnO reflection persists in this temperature

Table 4
Characteristics of the new reflections at 4 K for $Sr_2Mn_3As_2O_2$

Peak	$2\theta_{obs}$(deg)[a]	$2\theta_{calc}$(deg)[b]	Indices[b]	I_{rel}[c]	FWHM(deg)
a	17.11(3)			169(57)	0.42(8)
b	24.62(1)	24.65	(100)	8450(200)	—
c	35.18(1)	35.14	(110)	302(54)	0.43(4)
d	38.55(2)	38.52	(112)	181(47)	0.38(5)
e	45.60(4)			115(45)	0.38(8)

[a] Observed 2θ values have been corrected for the zero offset of 1.71°.
[b] Calculated 2θ values and indices are based on a magnetic cell $a_{MAG} = \sqrt{2}a$, $c_{MAG} = c$; $a_{MAG} = 5.863$ Å, $c_{MAG} = 18.810$ Å.
[c] Determined by computing integrated intensities; for (100) the range $26.2° \leq 2\theta \leq 33.2°$ was used.

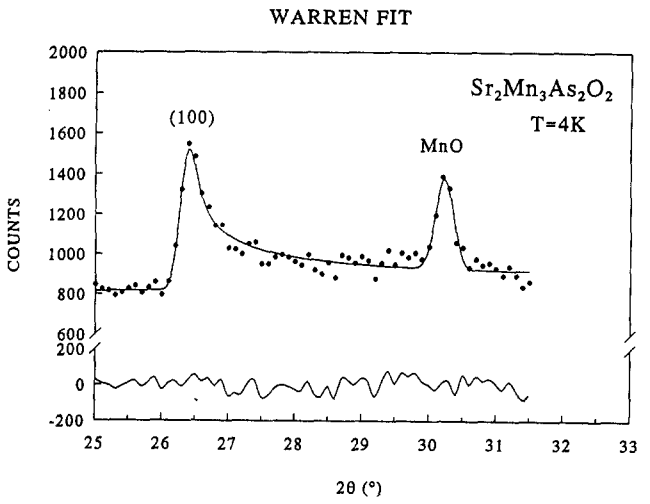

Fig. 10. Fit of the Warren function to the (100) magnetic reflection of $Sr_2Mn_3As_2O_2$. The correlation length is 540 Å.

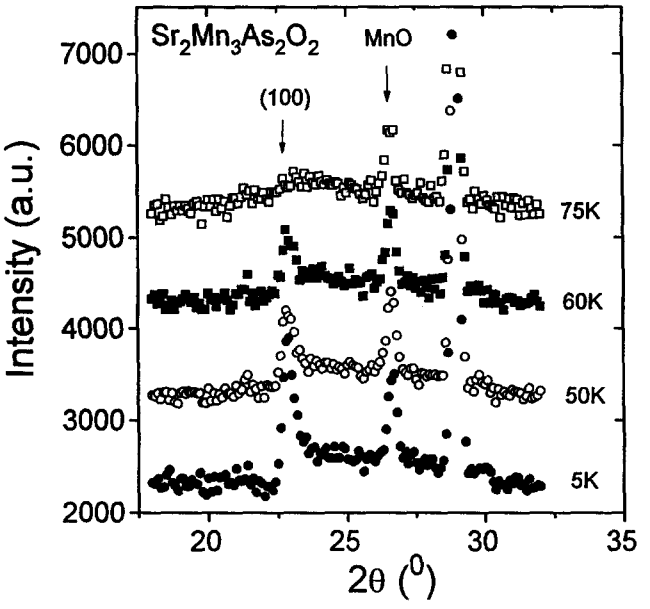

Fig. 11. Plot of the temperature dependence of the (100) magnetic reflection of $Sr_2Mn_3As_2O_2$. The (1/2 1/2 1/2) magnetic reflection due to MnO is also indicated.

range and vanishes above 100 K, which is consistent with the known T_c of 126 K.

Of the remaining reflections, which account for less than 10% of the total new scattered intensity at 4 K, it is difficult to draw clear conclusions. First, although two of these, d and e, can be indexed on the magnetic cell as the (110) and (112) reflections respectively, they show a different temperature dependence from peak a (the (100) reflection) disappearing between 100 and 150 K and the reflection condition, $h + k$ = even, is also different. Furthermore, the line widths of all these weak reflections are significantly greater than the resolution-limited width which spans the range from 0.260(1) to 0.264(1) in the 2θ interval of interest. Two possibilities are that these are all due to impurity phases, although most known simple compounds of Mn with Pn or O have magnetic transition temperatures, or that they signal a minor quasi-three-dimensional component of the predominant two-dimensional order.

4. Discussion

It is clear from the neutron data that the MnO_2^{2-} and $Mn_2Pn_2^{2-}$ layers behave as nearly independent magnetic systems and this is presumably due to the symmetry cancellation of the interaction between the two different layers. It has been mentioned that coupling between the nearest MnO_2^{2-} layers is also expected to cancel based on symmetry arguments, so one might expect no long range ordering within this lattice either; however, long range order is frequently observed for the body-centered tetragonal geometry and is attributed to coupling of each layer to the next nearest layer, which is favorable by symmetry [20]. Owing to the long distances between layers, intraplanar exchange is expected to be dominant for both Mn sublattices in $Sr_2Mn_3Pn_2O_2$. Interplanar coupling, via superexchange through several intervening atoms or via the dipolar interaction, is expected to be several orders of magnitude weaker than the intraplanar coupling [20], resulting in a strong two-dimensional character of the magnetism, which is consistent with susceptibility results [12,21].

The intraplanar exchange geometry for the two different layers is illustrated in Fig. 12. The Mn(1)–Mn(1) intraplanar exchange pathway involves a 180° Mn(1)–O–Mn(1) linkage, the ideal superexchange geometry. Mn(2)–Mn(2) intraplanar superexchange occurs through edge-shared $MnPn_{4/4}$ tetrahedra and there are two mechanisms by which this is likely to occur [22]. Superexchange can occur through the Mn(2)–Pn–Mn(2) geometry angle of 70–75° which would generally be expected to be weaker than the optimum 180° interaction. It is also possible to couple via delocalization exchange through direct overlap of Mn d orbitals. Consistent with this analysis, magnetic interactions within the $Mn_2Pn_2^{2-}$ layer appear to be more delocalized and covalent than those within the MnO_2^{2-} layer, as indicated by the fact that the low temperature moment for Mn(2) (3.4 μ_B) is smaller than that of the Mn(1) sublattice (4.2μ_B). Thus, the magnetic character is strongly influenced by the geometry of the sublattices. As the sublattices behave independently, it is useful to consider each sublattice independently and compare them with compounds which are structurally and electronically similar and whose magnetic properties have been investigated.

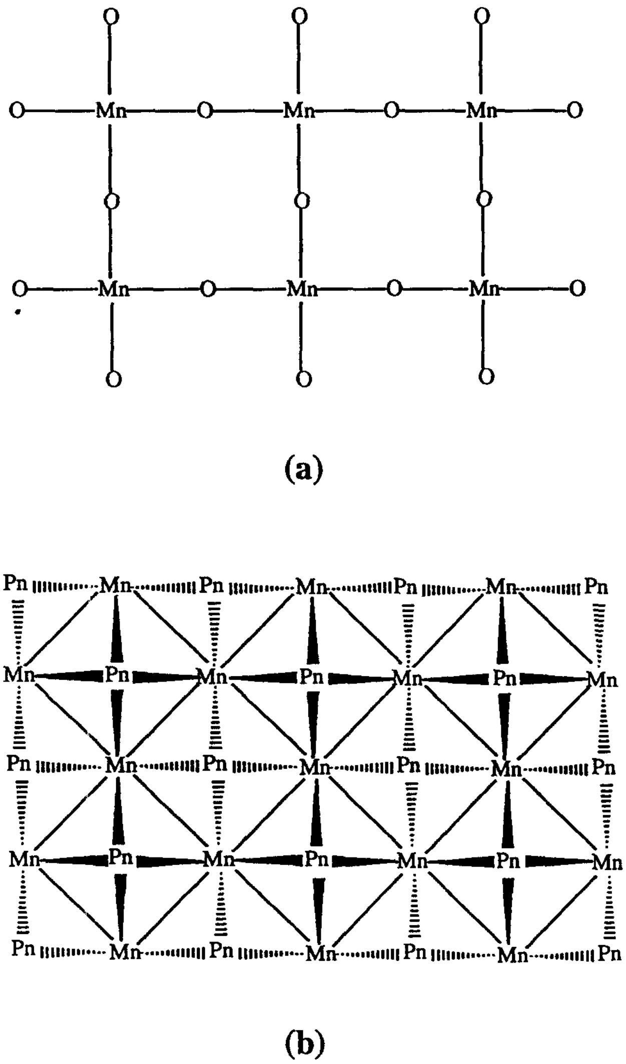

Fig. 12. Illustration of the bonding interactions which are expected to give rise to intraplanar superexchange in (a) the Mn(1) sublattice (MnO_2^{2-} layer) and (b) the Mn(2) sublattice ($Mn_2Pn_2^{2-}$ layer).

4.1. *Comparison of the Mn(2) sublattice to compounds containing $BaAl_4$-type units*

It has been pointed out that the Mn(2) sublattice ($Mn_2Pn_2^{2-}$ layers) in the $Sr_2Mn_3As_2O_2$ structure type is also found in the CeFeSi and $ThCr_2Si_2$ structure types. Caution should be exercised in the choice of systems for comparison, as in most cases involving the $ThCr_2Si_2$ structure types for example, it is not clear that the electronic structures are truly comparable with the valence precise pnictide oxide system [8,9]. Of the existing AMn_2X_2 compounds of the $ThCr_2Si_2$ structure type, only those with X = P, As, Sb and A = Ba qualify as true analogs, but only $BaMn_2P_2$ has been studied in any detail [18].

The CeFeSi-type compounds AMnPn (A = Li–Cs; Pn = P–Bi) also clearly qualify as valence precise analogs and fairly extensive data are available [23,24]. Some relevant data are collected in Table 5. First, note

Table 5
Comparison of interatomic distances and the ordered Mn(2) moments in compounds containing $BaAl_4$-type units

Compound	Mn(2)–Pn intralayer (Å)	Mn(2)–Mn(2) intralayer (Å)	$\mu(Mn^{2+})(\mu_B)$
$BaMn_2P_2$ [a]	2.331(3)	2.855(1)	4.2(1)
$Sr_2Mn_3As_2O_2$ [b]	2.574(1)	2.939(1)	3.4(1)
$Sr_2Mn_3Sb_2O_2$ [b]	2.741(1)	3.014(1)	3.5(1)
NaMnP [c]	2.482(4)	2.897(1)	3.63(5)
NaMnAs [c]	2.593(4)	2.969(1)	4.01(5)
NaMnSb [c]	2.766(9)	3.145(1)	4.08(6)

[a] Bond distances obtained from Ref. [25] and the magnetic moment from Ref. [18].
[b] Bond distances obtained from Ref. [11].
[c] Bond distances and magnetic moments obtained from Ref. [23].

that the ordered Mn^{2+} moments, as determined by neutron diffraction, are all significantly smaller than the free ion value of 5 μ_B expected for $S = 5/2$ and $g = 2.0$. This is a universal phenomenon in d-electron transition metal compounds and is attributed to delocation of the unpaired spin density via covalent mixing due to, in this particular case, Mn–Pn interactions. In these compounds, the short Mn–Mn distances (see Table 5) indicate that direct d–d interactions should also be considered, as mentioned previously. The local Mn–Pn geometries in $Sr_2Mn_3As_2O_2$ and $Sr_2Mn_3Sb_2O_2$ are remarkably similar to those for NaMnAs and NaMnSb with Mn–As and Mn–Sb distances essentially the same for both families of compounds; however, the $MnPn_4$ tetrahedra are slightly more distorted in the pnictide oxides.

Surprisingly, the structural similarities between the manganese pnictide layers in these families is not reflected in the magnetic moment. In AMnPn compounds, a clear correlation has been noted between increasing magnetic moment and increasing Mn–Mn intraplanar distance [24]. However, the Mn moments in the pnictide oxides are significantly smaller than in the AMnPn series for the same Mn–Mn distances. This suggests that the character of the $Mn_2Pn_2^{2-}$ layers is different (more covalent) in the quaternary pnictide oxides, apparently modified by electronic and lattice matching requirements of the MnO_2^{2-} layers.

A magnetostructural correlation which appears to be more universal concerns the critical temperature for long range magnetic order T_N and interplanar and intraplanar Mn–Mn distances. At first glance it may seem that the interplanar Mn–Mn distances would be most relevant to the three-dimensional ordering temperature, but this is not necessarily the case. For these layered materials it is likely that $J_0 \gg J'$, where J_0 is the intralayer exchange constant and J' is the interlayer exchange constant. A simple mean field theory argument suggests that $T_N \sim (\xi_{2D})^2 J/k$, where ξ_{2D} is the intraplanar AF correlation length which is an exponential function of temperature [26]. It is thus

argued that for the extreme situation in which $J_0 \gg J'$, as long as J' is finite, long range AF order will occur at some temperature, driven largely by the strong two-dimensional correlations. T_N would then depend strongly on ξ_{2D} which, in turn, will be strongly correlated with Mn–Mn intraplanar distances and less strongly on J', which correlates with interplanar distances. Consideration of Fig. 13, which collects data from the AMnPn and pnictide oxide series, indicates that T_N does indeed correlate with both intra- and interlayer distances and, as expected, the correlation with the former is stronger. At longer Mn–Mn distances there seems to be an approach to saturation in the T_N which suggests that J' is becoming less important. Both the previous observations are fully consistent with the qualitative consideration presented above.

4.2. The Mn(1) sublattice

Unfortunately, few Mn^{2+} oxides exist with the K_2NiF_4 structure type which would be good analogs for the Mn(1) sublattice; most such Mn^{2+} compounds are halide salts, such as K_2MnF_4 or Rb_2MnF_4, and so a detailed comparison of the sort done for the Mn(2) sublattice is not possible. A potentially interesting analog, La_2MnO_4, has been reported to have the tetragonal K_2NiF_4 structure, but no magnetic properties are known [27]. Therefore, discussion of the Mn(1) sublattice will focus mainly on a comparison of the neutron results for the two compounds, $Sr_2Mn_3Sb_2O_2$ and $Sr_2Mn_3As_2O_2$.

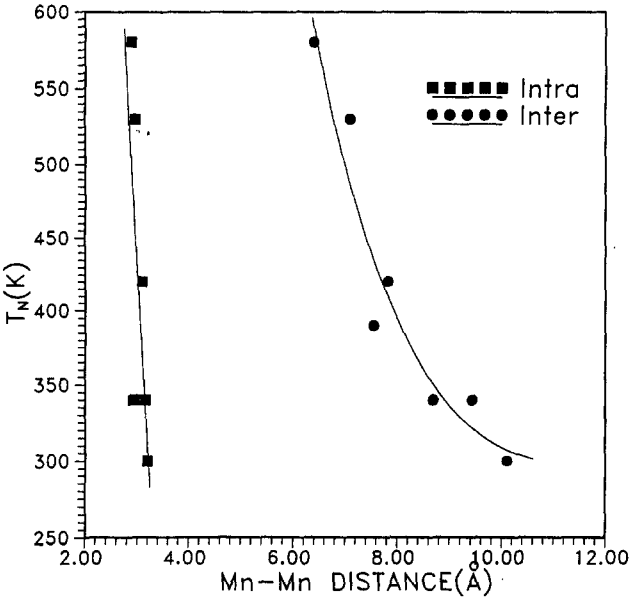

Fig. 13. Correlation of T_N with inter- and intralayer distances in AMnPn and $Sr_2Mn_3Pn_2O_2$. T_N values for AMnPn were estimated from existing data by extrapolation to high temperatures assuming an $S = 5/2$ Brillouin function dependence. Errors are estimated to be ±15 K which is roughly the dimension of the symbols used. The lines indicate the trend in the data.

Three-dimensional long range AF order on the Mn(1) lattice is found only for $Sr_2Mn_3Sb_2O_2$ and the magnetic structure is identical to that of K_2NiF_4. The relatively low ordering temperature of 65 K reflects the symmetry cancellation existing for the Mn(1)–Mn(1) and Mn(1)–Mn(2) interactions, as previously pointed out. Remarkably, three-dimensional order is never established for $Sr_2Mn_3As_2O_2$ on the Mn(1) sites, at least above 4 K, as evidenced by the Warren line shape observed, although the in-plane correlation length attains the rather large value of about 500 Å. As indicated in the discussion of the Mn(2) magnetic sublattice, long range three-dimensional ordering within a sublattice is expected to occur when the two-dimensional correlation length becomes sufficiently long (greater than 1000 Å in the case of K_2NiF_4 [28]); thus, it is not impossible that three-dimensional order will set in at lower temperatures in $Sr_2Mn_3As_2O_2$. Nevertheless, the very wide range over which two-dimensional correlations are manifest for the Mn(1) sublattice of $Sr_2Mn_3As_2O_2$ is in sharp contrast to $Sr_2Mn_3Sb_2O_2$ and to other two-dimensionally coupled systems [28,29]. Typically, two- and three-dimensional ordering occur at nearly the same temperature. Notable exceptions are the oxide superconductors $DyBa_2Cu_4O_8$ and $Dy_2Ba_4Cu_7O_{15}$, which, analogous to $Sr_2Mn_3As_2O_2$, demonstrate a Warren lineshape for the scattering due to the rare earth layers and show no tendency towards long range three-dimensional order [30]. The magnetic behavior of $Sr_2Mn_3As_2O_2$ suggests the presence of magnetic frustration opposing long range order in this particular compound. The source of this unique behavior for $Sr_2Mn_3As_2O_2$ relative to $Sr_2Mn_3Sb_2O_2$ (and other compounds of the K_2NiF_4 structure type) is unclear, unless it is due to small structural differences between the two compounds, a possibility which is discussed in detail elsewhere [21].

Acknowledgements

We thank G. Liu for discussions and assistance in obtaining some of the neutron data sets for $Sr_2Mn_3As_2O_2$ and R. Donaberger and I. Swainson (AECL) for considerable assistance in obtaining the neutron data at DUALSPEC. S. Brock gratefully acknowledges a U.C. Dissertation Year Fellowship. The research at U.C. Davis is supported by NSF, Division of Materials Research, DMR-9201041, and the donors of the Petroleum Research Fund administered by the ACS. The Natural Science and Engineering Research Council of Canada is acknowledged for support of the work at McMaster and for infrastructure support of the DUALSPEC facility.

References

[1] J. Hauck and K. Mika, *Int. J. Mod. Phys. B, 7* (1993) 3423.
[2] E. Parthé and B. Chabot, in K.A.J. Gschneidner, Jr. and L. Eyring (eds.), *Handbook on the Physics and Chemistry of Rare Earths*, Vol. 6, Elsevier, New York, 1984, pp. 113–334.
[3] T. Siegrist, H.W. Zandbergen, R.J. Cava, J.J. Krajewski and W.F. Peck, Jr., *Nature, 367* (1994) 254.
[4] E. Mörsen, B.D. Mosel, W. Müller-Warmuth, M. Reehuis and W. Jeitschko, *J. Phys. Chem. Solids, 49* (1988) 785.
[5] M. Reehuis and W. Jeitschko, *J. Phys. Chem. Solids, 51* (1990) 961.
[6] M. Reehuis, T. Vomhof and W. Jeitschko, *J. Less-Comm. Met., 169* (1991) 139.
[7] M. Reehuis, W. Jeitschko, M.H. Möller and P.J. Brown, *J. Phys. Chem. Solids, 53* (1992) 687.
[8] A. Szytula and J. Leciejewicz, in K.A.J. Gschneidner and L. Eyring (eds.), *Handbook on the Physics and Chemistry of Rare Earths*, Vol. 12, Elsevier, New York, 1989, pp. 133–211.
[9] B. Malaman, G. Venturini, R. Welter and E. Ressouche, *J. Alloys Comp., 210* (1994) 209.
[10] G. Venturini, R. Welter, E. Ressouche and B. Malaman, *J. Alloys Comp., 210* (1994) 213.
[11] E. Brechtel, G. Cordier and H. Schäfer, *Z. Naturforsch B, 34* (1979) 777.
[12] N.T. Stetson and S.M. Kauzlarich, *Inorg. Chem., 30* (1991) 3969.
[13] S.L. Brock and S.M. Kauzlarich, CHEMTECH, *25* (1995) 18.
[14] S.L. Brock and S.M. Kauzlarich, *Comm-Inorg. Chem., 4* (1995).
[15] J. Rodriguez-Carvajal, FULLPROF, Institute Laue–Langevin, unpublished.
[16] A. Bondi, *J. Phys. Chem., 68* (1964) 441.
[17] S.L. Brock, J.E. Greedan and S.M. Kauzlarich, *J. Solid State Chem., 109* (1994) 416.
[18] S.L. Brock, J.E. Greedan and S.M. Kauzlarich, *J. Solid State Chem., 113* (1994) 303.
[19] B.E. Warren, *Phys. Rev., 59* (1941) 693.
[20] L.J. de Jongh and A.R. Miedema, *Adv. Phys., 23* (1974) 1.
[21] S.L. Brock and S.M. Kauzlarich, *J. Alloys Comp.*, submitted for publication.
[22] J.B. Goodenough, *Magnetism and the Chemical Bond*, Interscience, New York, 1963.
[23] W. Bronger, P. Müller, R. Höppner and H.-U. Schuster, *Z. Anorg. Allg. Chem., 539* (1986) 175.
[24] R. Müller, M. Kuckel, H.-U. Schuster, P. Müller and W. Bronger, *J. Alloys Comp., 176* (1991) 167.
[25] A. Mewis, *Z. Naturforsch. B, 35* (1980) 141.
[26] L.J. de Jongh, in L.J. de Jongh (ed.), *Magnetic Properties of Layered Transition Metal Compounds*, Kluwer, Dordrecht, 1990, p. 19.
[27] H.W. King, K.M. Castelliz, G.J. Murphy and A.S. Rizkalla, *J. Can. Ceram. Soc., 55* (1986) 10.
[28] R.J. Birgeneau, H.J. Guggenheim and G. Shirane, *Phys. Rev. B* 1 (1970) 2211.
[29] R.J. Birgeneau, H.J. Guggenheim and G. Shirane, *Phys. Rev. B* 8 (1973) 304.
[30] J.W. Lynn, *J. Alloys Comp., 181* (1992) 419.